Effects of the solution and first aging treatment applied to as-built and post-HIP CM247 produced via Laser Powder Bed Fusion (LPBF)

Journal of Alloys and Compounds 905 (2022) 164213

Contents lists available at ScienceDirect

Journal of Alloys and Compounds

journal homepage: www.elsevier.com/locate/jalcom

Research Article

Effects of the solution and first aging treatment applied to as-built and post-HIP CM247 produced via laser powder bed fusion (LPBF)

E. Bassini[a,c,*], A. Sivo[a,c], P.A. Martelli[a,c,d], E. Rajczak[a,c,d], G. Marchese[a,c], F. Calignano[b,c,d], S. Biamino[a,c,d], D. Ugues[a,c,d]

[a] Politecnico di Torino, Dip. Scienza Applicata e Tecnologia (DISAT), Italy
[b] Politecnico di Torino, Dip. Ingegneria Gestionale e della Produzione Industriale (DIGEP), Italy
[c] Centro Interdipartimentale IntegratedAdditive Manufacturing IAM@PoliTO, Italy
[d] Consorzio Nazionale della Scienza e Tecnologia dei Materiali (INSTM), Italy

ARTICLE INFO

Article history:
Received 20 December 2021
Received in revised form 7 February 2022
Accepted 11 February 2022
Available online 15 February 2022

Keywords:
Selective laser melting
CM247 LC
Nickel based alloys
Low weldable alloys
Additive manufacturing

ABSTRACT

In this work CM247LC, a low weldable Ni-Based alloy, was produced using selective laser melting (SLM). Despite the initial process parameter optimization, the low defect volume fraction was still uncompliant with manufacturing standards. This condition is principally caused by the high γ' volume fraction which strongly affects the alloy weldability. Nonetheless, a crack free condition was eventually achieved applying a γ'-sub-solvus Hot Isostatic Pressing Cycle (HIP) which lowered the defects fraction down to 0.04%. The HIP cycle also demonstrated to play an important role in the stabilization of the microstructure, considerably limiting the carbides coarsening during the following heat treatment. Apart from the effectiveness of the healing process brought by HIP, the material microstructure still needs an optimization process which will be described along this paper. In fact, the Initial microstructure obtained after the printing process (the as-built condition) as well as the one obtained after HIP (post-HIP) won't meet the desired requirements. Namely, the dendritic and γ' free microstructure of the as-built material or the one with coarse and disordered particles obtained right after HIP, still need a tailored homogenization process. This paper will show how the combined effect of the solution and first aging treatment will profoundly alter the γ' precipitation. More specifically, here, a new heat treatment recipe was developed to promote the precipitation of ordered cuboidal primary γ' so as to improve creep and high temperature fatigue resistance. Moreover, the use of a γ' super-solvus temperature allowed to achieve a γ' volume fraction as high as 73% reducing its average size to 520 nm. At the same time, such heat treatment caused a profound alteration of the crystalline structures of the material promoting a general grain coarsening and the formation of equiaxial grains.

1. Introduction

CM247 LC is a well-known nickel-based superalloy which is typically used to produce jet engine turbine blades and in power plants as well. The reason for this derives from its mechanical properties stability at high temperatures as well as its high resistance to oxidation. According to the work of MacDonald [1] this alloy can withstand temperatures ranging between 870 and 982 °C.

Similarly to other Nickel based alloys, also CM247 LC consists of an austenitic matrix (γ) reinforced via precipitates: Ni3(Al-Ti) γ' and carbides [2] being the first the main reinforcing element of the material [3,4]. Carbides, on the other hand, typically are in the form of M_6C or $M_{23}C_6$ depending on their nucleation site and they may contain Ti, Cr, Hf, W, Nb or other carbide former elements [2,5,6]. Some authors such as Yang affirm that they may have a positive effect increasing creep resistance [2] while others affirm that they may cause premature failure due to their incipient melting. Nevertheless, their fraction, shape and distribution must be controlled via tailored heat treatments avoiding the formation of thick networks at the grain boundaries [7].

Naturally, manufacturing complex shaped components with Ni-based alloys such as Rene 80 or CM247 become difficult and expensive when traditional techniques are applied. This is one of the root reasons for progressively moving to more recent techniques, such as the laser powder bed fusion (L-PBF), which has proved to be extremely effective for producing γ'' reinforced alloys as IN718,

* Correspondence to: Politecnico di Torino, Dip. Scienza Applicata e Tecnologia (DISAT), corso duca degli abruzzi 24 10129 Torino Italy.
E-mail address: emilio.bassini@polito.it (E. Bassini).

https://doi.org/10.1016/j.jallcom.2022.164213
0925-8388/

IN625, or Hastelloy X [6,8–12] or non nickel-based alloys [13]. Conversely, CM247 LC is reinforced with a very high γ' volume fraction, making this material difficult to be processed via laser melting [14]. Marchese evidenced similar difficulties also in his work on IN939 whose low weldability was addressed with a process parameter optimization [15]. Donachie, clearly demonstrated that many cracks were likely to form after welding of CM247 LC due to liquation cracking or post-weald heat treatment (PWHT) [16]. Also Carter, in his review [17], deeply investigated CM247 LC low weldability. One of the most relevant conclusions is that the flaw density may be drastically reduced using a proper process parameter optimization during SLM. Grange et al. [18] examined the correlation between the melt pool width, the grain size and the occurrence of solidification cracking. They demonstrated that narrowing the melt pool size may subdue hot cracking in Ni-based superalloys. Bidron et al. [19] suppressed crack defects using a pre-heating temperature of 1050 °C. Gerstgrasser et al. [20] concentrated on focus shift on SLM-processed CM247LC. They put a stress on the laser beam diameter as a crucial factor that allows to re-molten cracks and obtain a high quality, dense alloy.

Furthermore, the population of defects such as pores, cracks or lack of fusion may be even more reduced using the Hot Isostatic Pressing [21–24]. HIP application also causes strong microstructural changes from the SLM as-built state to the post-HIP one. The microstructure of the SLM material is typically made of colonies of differently oriented dendrites due to the rapid solidification of the melt after the laser scan. The heat flow and the cooling rates involved are so high that primary dendrites grow towards the center of the melt pools and formation of second order branches are practically suppressed. Due to the layer by layer manufacturing process, grains in SLM materials can easily come across several melt pools as demonstrated in the work of Calandri [10]. Dendritic colonies result all oriented along the direction characterized by the strongest heat flow i.e. the building direction (z-direction) [21]. First of all, HIP will lead to the formation of γ' whose precipitation was hindered by the extremely rapid cooling rate of the SLM process. The size and shape of the γ' particles will be affected by the cooling rate after hot isostatic pressing as well. Slow cooling rate will lead to the formation of coarse particles characterized by the so called fan-like shape as demonstrated by Bassini for a different Nickel alloy [25]. On the other hand, the typically z-oriented microstructure of SLM material can be either retained or substituted with an equiaxial microstructure depending on the alloy used [21,26]. In this work, the homogenization process was applied to the material in two metallurgical conditions, i.e. in the as-built condition and after the HIP process. This was extremely useful to separate the microstructural effects of each of part of the heat treatments. Most importantly, it was evidenced that HIP has a positive effects in controlling the coarsening of the carbides of the SLM material during the homogenization treatment. Regarding this, Chao showed that HIP refined the script-like MC carbides of a cast CM681LC into round $M_{23}C_6$ carbides[27]. While others focused on carbides evolution in a NNSHIP Astroloy as a consequence of different heat treatments application [23].

Noteworthy, the microstructural sensitivity towards heat treatments of an SLM material is completely different with respect to that of traditional manufactured ones. So, making dedicated studies about this topic is extremely important.

Independently of the manufacturing process, the heat treatment of CM247 LC is made of different stages. The first one is performed at the highest temperature, above 1200 °C and conventionally is called homogenization. The following heat treatment stages allow to achieve the proper carbide distribution as well as providing the basis for a suitable γ' precipitation. More specifically, according to Baldan and Wang the γ' solvus for cast and SLM are different and located between 1220 and 1260 °C[28,29].

The heat treatment will strongly influence the average size and fraction of γ' precipitates which in this material appears as cuboidal particles due to the lattice mismatch between the particles and the matrix [30,31]. Normally cast CM247 LC is known for having a γ' volume fraction close to 65% as assessed by Kim [32]. Differently from other Ni-based alloys such as Astroloy [33–35] which shows a tri-modal distribution, CM247 LC reinforcing system consist of only two families of precipitates namely primary and secondary γ'. In traditionally manufactured samples primary and secondary gamma prime measure around 300 and 35 nm respectively [31]. Such precipitates, as long as they remain stable, are extremely effective in preventing the dislocation movements as demonstrated by Pollock [36] in her work.

The core reason for focusing only on the solutioning and first aging cycle is because these steps are crucial for determining the final microstructural and mechanical properties of the material. Conversely the low temperature steps e.g. the second aging will have only a slight impact. This was demonstrated in many literature works for SLM materials different from CM 247LC for example in the work of Calandri [37] for IN718. Xu came to similar conclusions on a 60 vol% γ' reinforced alloy called MAD542; in his work clearly explains the importance of the solution treatment to achieve the highest γ' volume fraction[38]. Also for HIPPed Astroloy, the solution temperature dramatically changed the γ' morphology and volume fraction [25]. In other words, γ' precipitation must be optimized to maximize mechanical properties of a nickel-based alloy, and this task may be accomplished only tailoring the solution treatment as described by Kakehi [39]. At the same time, also the volume fraction of γ' strongly alters the ability of the alloy of withstanding high temperatures, more specifically, Khafri [40] which worked on Inconel 738 C, reported longer creep life in samples having higher γ' fractions.

It is apparent that obtaining the correct size and fraction of γ' precipitates will be of extreme importance to obtain the best mechanical properties and stability at high temperature. For this reason, the following study will deal with the microstructural effects of the homogenization/solutioning and first aging treatments towards CM247 LC, underlining how to maximize the γ' volume fraction, improving its shape and average size, setting the basis for an optimized and complete heat treatment recipe once the second aging will be provided. In this paper, also the starting metallurgical state will be kept into account, showing whether the application of the HIP treatment may alter the γ' precipitation and the carbide population.

2. Materials and methods

2.1. Sample preparation

The CM247LC samples were printed using an EOS M270 Dual mode version working with high purity Argon starting from pre-alloyed inert gas atomized powders provided by Praxair whose chemical composition according to manufacturer datasheet is indicated in Table 1.

Powders were tested also for determining the apparent density according to ASTM B212 as well as the flow ability according to ASTM B213 obtaining as a result 4.63 ± 0.01 g/cm^3 and 12.9 ± 0.2 s/50 g, respectively. Finally, the particle size distribution of the powder was assessed and D10, D50 and D90 resulted 9.7, 19.4 and 33.3 μm respectively determined via laser granulometry. The samples used

Table 1
CM 247 LC powders chemical composition.

Cr [%]	Co [%]	Mo [%]	W [%]	Ta [%]	Al [%]	Ti [%]	Hf [%]	Zr [%]
8.0	9.3	0.5	9.7	3.6	5.2	0.8	1.7	0.01

Table 2
Element composition of CM247 powder and as-built (SLM) product.

Elements	Raw powder	As-built
C (%)	0.083 (± 0.001)	0.068 (± 0.001)
S (ppm)	4.79 (± 0.08)	13.6 (± 0.97)
O (%)	0.014 (± 0.002)	0.0067 (± 0.0001)
N (%)	0.0036 (± 0.0002)	0.0049 (± 0.00002)
H (ppm)	7.89 (± 1.38)	2.37 (± 0.42)

were 15 mm cubes printed on a low alloyed carbon steel platform. The samples were built using stripes scanning strategy with a laser rotation of 67° among each consecutive layer of powders. The content of interstitial elements (C, S, O, N and H) of densified materials was determined and compared with the results obtained from raw powders. C and S were determined by oxygen combustion in Leco CS 744 whereas O, N and H values were determined by inert gas fusion in Leco ONH 836. The obtained results are reported in Table 2.

2.2. Thermal analysis

The thermal analysis was performed using Setaram TG 16.18 instrument in the temperature range of 50–1400 °C with a scan rate of 10 °C/min. Both heating and cooling ramp were recorded but only the heating ramps are shown being more noteworthy. The analyses were performed on a as-built and post-HIPped samples in order to compare them accordingly from a thermodynamic point of view and evidence if the two metallurgical condition show a different γ' solvus interval.

2.3. Metallurgical observation

Firstly, the sample flaw density (cracks and pores) after production was assessed on cubes cross section after a traditional metallographic preparation. More precisely, samples were cut along the z-y plane and embedded in resin. The samples were then ground using SiC sandpapers from 180 down to 1200 grit. Polishing, on the other hand, was obtained using diamond pasted from 6 to 1 µm. Finally, colloidal Silica was used to obtain the correct surface finishing for observation at the optical microscope. At this stage, no chemical etching was used. A total of 15 pictures per sample were taken at 50X magnification for a total observed area of 38 mm^2. The optical microscope was a Leica MEF4 with a picture resolution of 0.914 µm/pixel. The pictures where then enhanced in contrast and processed via ImageJ in conjunction with a python compiled software which was able to distinguish cracks from pores giving separate results for these two features. The other half of the samples were prepared in the same way but etched with aqua regia i.e. a 1:3 part of Nitric and Hydrochloric acid mixture for ca. 10 s. The γ' structural change was observed using an electrolytic etching. The 20% H_3PO_4 water solution, with an applied voltage of 5 V allowed to consume the γ matrix exposing the reinforcing particles. Depending on the metallurgical state, the etching time was varied from 5 to 20 s. This further step was considered particularly effective for revealing the γ' particles using the Scanning Electron Microscope (SEM), a Zeiss EVO15.

2.4. HIP and heat treatments set up

The Hot Isostatic Pressing of the sample (half batch) was performed within a Quintus QIH 15 L equipped with a Molybdenum furnace. The HIP process was performed in a sub-solvus regime increasing temperature and pressure at the same time. Despite the HIP was equipped with a Uniform Rapid Cooling (URC) module, the samples were naturally cooled to room temperature with at 15 °C/min rate calculated from the HIP temperature to 400 °C.

The heat treatment was conducted in a low-pressure furnace TAV mini jet. The solutioning/homogenization treatment and the first aging were separated by a gas quench. The Nitrogen pressure was regulated to obtain a cooling rate of 50 °C per minute from the solution temperature to that of the first aging. Solution Time was fixed and equal to 2 h, as well as the first aging temperature and time being 1080 °C and 4 h respectively. The solution treatment was performed at different temperatures starting from 1205 °C up to 1245 °C.

2.5. Hardness assessment

The hardness was measured performing 10 indentation per sample with a micro Vickers hardness machine leica MICROVHT1200 applying 300 g for 15 s.

2.6. Microstructural assessment via EBSD

A focused ion beam-scanning electron microscopy (FIB-SEM, TESCAN S9000G, Tescan) equipped with an electron backscatter diffraction (EBSD) detector was employed to study the degree of recrystallization under heat treatments. The polished specimens were tilted by 70◦ and scanned at 20 kV, analyzing the building direction (z-axis).

3. Results and discussion

3.1. DSC thermograms

Fig. 1 shows the DSC signals of as-built and post-HIP samples aiming to identify the γ' solvus temperature range thus outlining the actual heat treatments.

The thermogram shows a sharp deviation from the base line in the 1247–1265 °C temperature range which was attributed to the γ' solvus in accordance with other works found in literature[1,41]. According to the above picture, the HIP sample shows a slightly broader solution interval. This could be related to the different state of the precipitates within the matrix, in the two metallurgical states and probably an easier dissolution of γ' in the HIP sample. Together with the γ' solvus temperature range, also the MC dissolution temperature and the alloy solidus and liquidus points were identified. This was also extremely useful to set the limits for the following heat treatments.

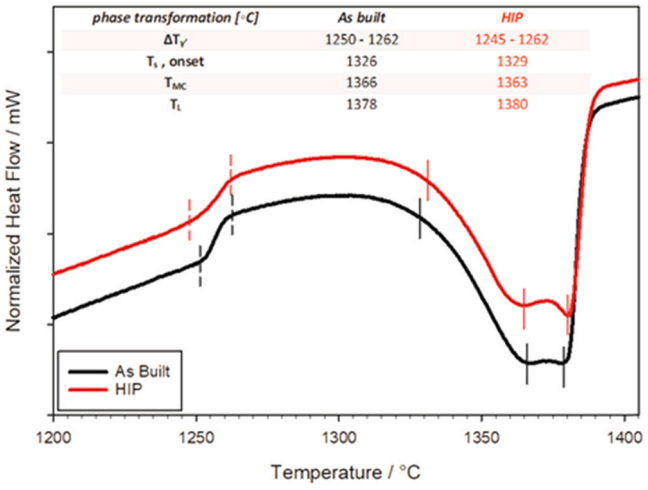

Fig. 1. Comparison of DSC thermograms for CM247 lc in as-built (black) and after HIP (red). (For interpretation of the references to color in this figure legend, the reader is referred to the web version of this article.)

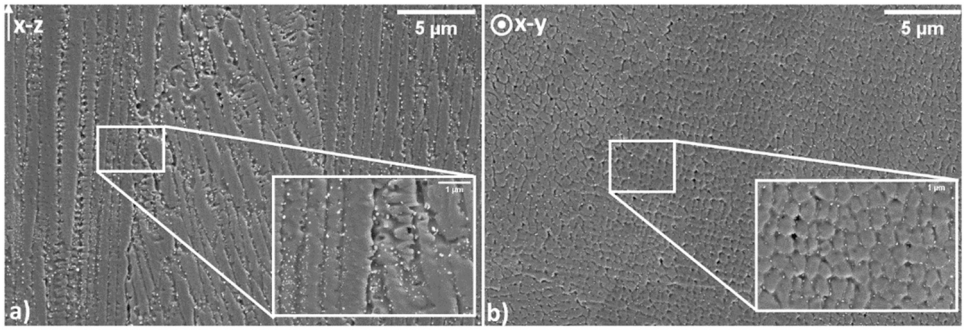

Fig. 2. Microstructures of the SLM CM247 lc observed in the x–z plane (a) and in the x–y plane (b) in the as-built condition. the dendrites are parallel to the building direction (left) and observable in their cross section (right).

3.2. Microstructural assessment

3.2.1. The as-built microstructure

As debated in the introduction, the microstructure of an SLM material is drastically different from the as cast one. Fig. 2 shows the dendritic microstructure in the XY and XZ planes.

The resulting microstructure is different in the two metallurgical orientations. The one along the building direction shows elongated dendrites with barely visible secondary branches. Very small carbides rich in Hf are clearly visible in the interdendritic regions, where segregation phenomena are more likely to occur. The extremely small size of carbides makes EDS analysis not very significant, but their formulation and stoichiometric formula was studied in depth in several studies and in particular in that of Divya [42]. The dendrites appear to be parallel to the strong heat flux provoked by the laser beam processing.

By observing the same sample in the x-y direction the dendrites are cut in their cross section thus a cellular microstructure become immediately recognizable. As previously described, the interdendritic regions are enriched in segregated elements, leading to Hf carbides stabilization as also shown in the work of Baldan [28]. Noteworthy is that the γ' precipitates are not visible, presumably because of the extremely high cooling rate which characterize the solidification of SLM components.

3.2.2. The post HIP microstructure

Fig. 3 shows samples in the two metallurgical orientations after being HIPped.

First of all, the HIP treatment completely eliminated the dendritic microstructure which was substituted with a more homogeneous one. Despite this, two features from the as-built state were inherited: grains still show an elongated shape, parallel to the building direction and several primary carbides, formed in the interdendritic regions are still visible, making the grain boundaries more recognizable. In the x-y section, γ' appear smaller and almost circular, indicating that also the precipitates assumed an elongated shape similar to that of a three-dimensional ellipsoid. Primary carbides are located at grain boundaries and organized in large irregular pattern similar to circumferences with a diameter that change point to point. Differently from the X-Z sample, several small carbides were found also in the intragranular region. Considering that pressure applied during HIP won't modify the γ' prime precipitation behavior, this microstructure may be considered a good approximation of a solely sub-solvus solutioned slowly quenched samples. Thus, this condition was not investigated separately. Focusing on the HIP microstructure achieved, some features appear evident: despite the overall microstructure looks more uniform, the precipitated γ' is still not acceptable. The slow cooling rate and the temperature used after HIP promoted the growth of the particles rather than their nucleation. As a result, γ' didn't develop the expected ordered cubic shape. As a consequence of this, overall mechanical properties still will not be compliant with the expected requirements. For this reason, the homogenization treatment become necessary and its effect will be discussed in the following sections.

Focusing more on the healing effect of the treatment, HIP drastically reduced the retained porosity and the degree of flaws in the treated samples. The observation of the samples via optical microscope demonstrates how the majority of the defects were removed. Hip was extremely effective to eliminate the inner porosity or cracks while those connected to the sample surface were not healed. Fig. 4a) and b) shows a comparison between the as built and the post hip conditions. The fraction of defects was calculated separately for cracks and pores (in the as-built condition). Initially these values were 0.22% and 0.18%, respectively. The HIP treatment reduced these flaws fraction down to 0% and 0.04%, respectively. As can be observed, the short solidification cracks are the more evident and frequent defect type. After HIP cracks are completely healed; Only pores with a diameter smaller than 5 µm were detectable. HIP leads to the elimination of the defects with highest stress intensity factor i.e. cracks which are characterized by a sharp tip radius. At the end of

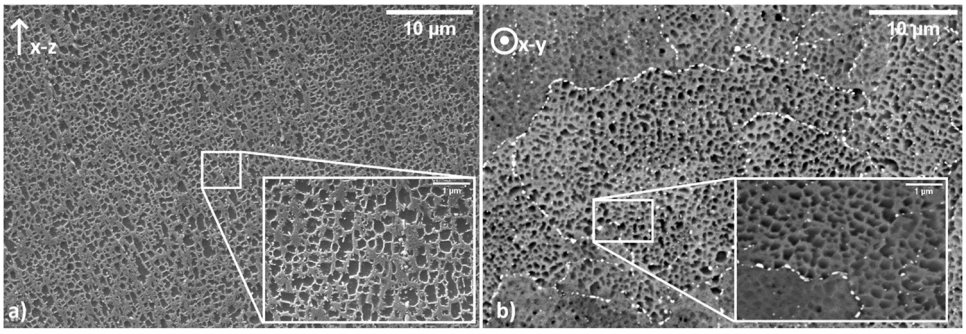

Fig. 3. Microstructures of the SLM CM247 lc observed in the x–z plane (a) and in the x–y plane (b) after being HIPped.

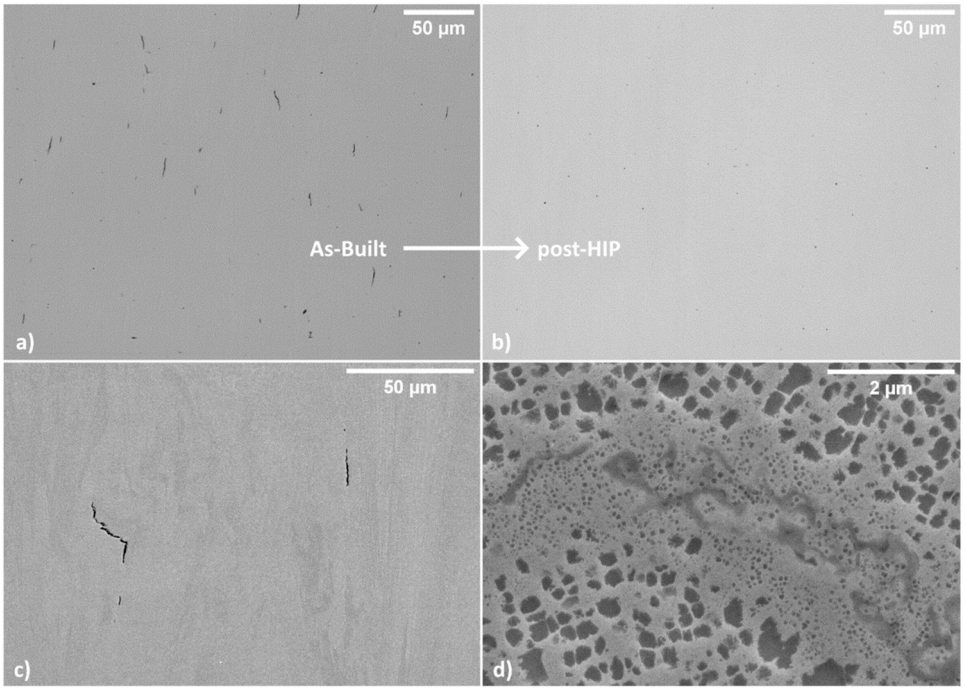

Fig. 4. the application of the HIP treatment closes the majority of the defects. Pictures a) and b) were taken with an optical microscope and clearly demonstrate the elimination of the cracks. Only small pores are retained. Picture c) shows cracks using the SEM, while d) shows how a crack looks like after its closure due to HIP application.

the healing treatment only round and very small defects will remain in the material which will be better tolerated when stresses are applied. Using the field emission electron microscope, it was possible to assess the microstructure of post-hipped sample in detail. As shown in Fig. 4d) the pores or cracks have been closed thanks to solid state diffusion making the resulting microstructure different with respect to that of the surroundings. The region in fact appears slightly depauperated in γ' fraction and the precipitates observable are considerably smaller than all the other away from the healed flaw. The reason for this type of feature may be probably ascribed to the different chemical composition obtained after the strong diffusive movements of atoms under the driving force of constitutional gradients. Despite this, such defects will be eliminated after the homogenization treatment.

3.2.3. Solutioning treatment and first aging cycle

At this point, to achieve the best possible microstructure the solution and first aging treatments were applied. Solutioning is the most important part of the treatment to determine the final size and shape of the precipitated γ'. For this reason, only the solution treatment temperature was progressively increased keeping all the other parameters (solution holding time, cooling rate and first aging) fixed. As described in the next paragraph the solution treatment temperature investigated were 1205, 1215, 1230 and 1245 °C respectively. More precisely, the solution and first aging treatment were applied to the material in two different starting metallurgical conditions: As-built and post-HIP samples respectively. This was considered useful to better evidence the differences at microstructural level brought by the HIP, since in this case, γ' has already precipitated within the austenitic matrix.

3.2.4. Heat treatment cycle applied to as-built samples

The application of the cycle descripted above, without HIP, didn't reduce the amount of defects from the as-built state, making this choice of little interest especially from an industrial point of view. For this reason, only the lowest and the highest solution temperatures were investigated here, i.e. 1205 and 1245 °C respectively. Nevertheless, this experiment was scientifically interesting to better separate the effects brought by the solution step by itself on a material which was characterized by a dendritic microstructure and totally γ' free.

Fig. 5 shows two As-built samples after solution and aging treatment. The solution treatment was able to eliminate the dendritic features and γ' precipitated. The former primary dendritic boundaries are strongly highlighted by carbide precipitation. As will be further described later, the shape of γ' after the heat treatment

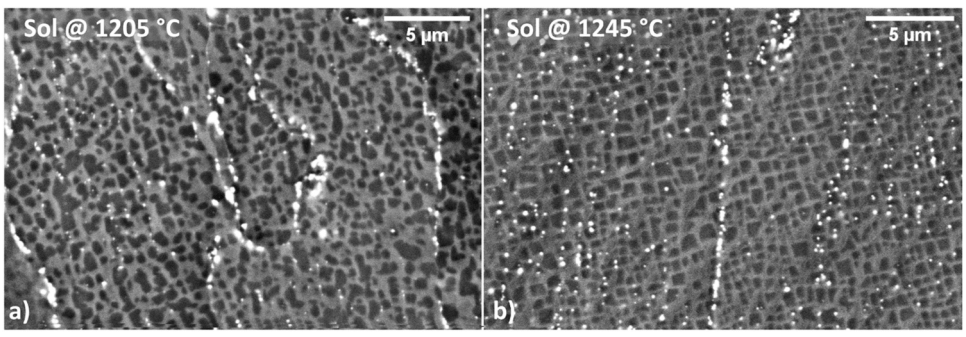

Fig. 5. As built samples subjected to the heat treatment cycle: a) shows the material solutioned at 1205 °C while b) the one solutioned at 1245 °C.

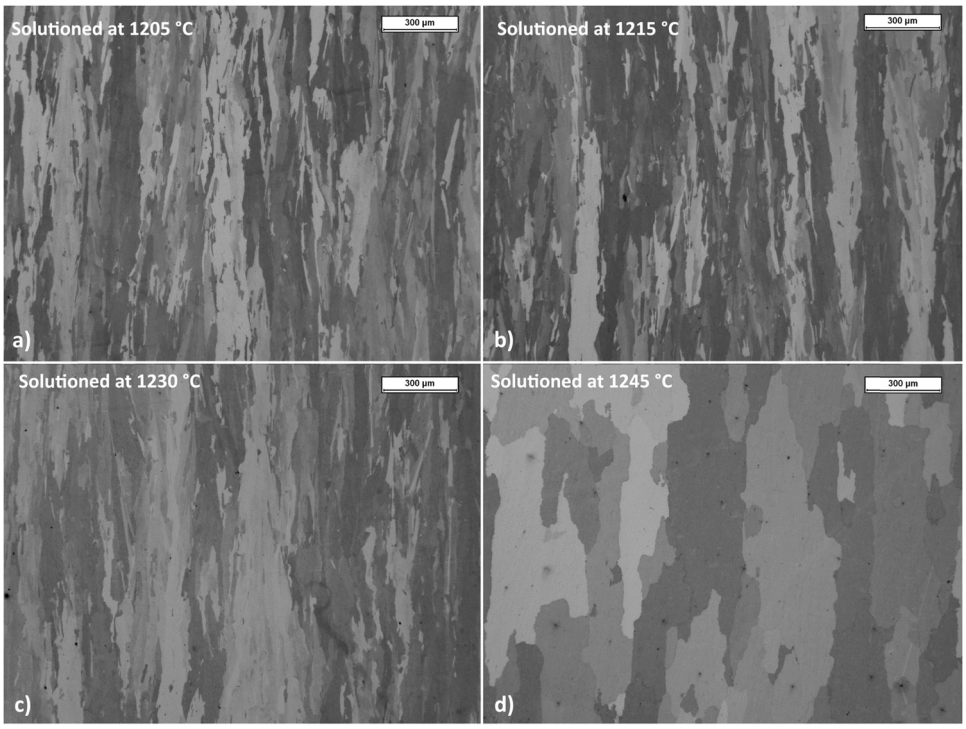

Fig. 6. Effect of the solution temperature on grain growth. The size increase becomes evident only when γ' solvus temperature is overcome.

cycle changes drastically depending on the chosen solutioning temperature. By solutioning at lower temperature, γ' is not ordered cuboidal. Its shape is rather elliptical or rectangular. This means that by holding at a sub-solvus temperature, despite a proper cooling rate was applied (i.e. 50 °C/min), the precipitation of the intermetallic cannot be shape-wise controlled. The following first aging treatment promote the growth and a further precipitation of γ' but cuboidal particles cannot be achieved. Differently from previous case, a fine cuboidal and well-organized precipitation was obtained as the γ' solvus is overcome. The γ' particles sides often share the same orientation with the containing columnar grains giving a general sense of preferential orientation of the particles. Finally, carbides were found located both at the former dendritic boundaries and in the core of the grains.

3.2.5. Heat treatment cycle applied to post-hip samples

This time the previously described heat treatment cycle was applied to the HIPped samples. The solution temperature was progressively increased from 1205° to 1245°C again without changing all the others parameters. Fig. 6 shows the effects of the solution temperature on grain coarsening. As can be seen, grain size is stable until temperature is lower or equal to 1230 °C. As the γ' solvus is overcome, as for 1245 °C, the grain coarsening is evident. Apparently, as the pinning effect of γ' located at the grain boundaries is vanished after their dissolution, the grains are free to spread. This effect is much more pronounced in the x or y direction while is quite limited in the z one. At lower temperatures i.e. between 1205 and 1230 °C there is almost no grain growth as discussed in the next paragraph. Grains measure 27 ± 9 and 103 ± 70 µm in the x and z direction respectively when solutioning is performed at 1205 °C while they growth to 45 ± 23 and 114 ± 87 µm respectively increasing the solutioning temperature up to 1230 °C. Conversely, after solutioning at 1245 °C, the grains in the z direction measure 371 + /- 60 µm and 138 + /- 12 in the opposite one.

On the other hand, Fig. 7 shows how the solutioning temperature affects the overall microstructure focusing on the precipitates. As the temperature increases, the final γ' obtained is smaller and progressively with a higher volume fraction. Up to 1230 °C the temperature is still low to obtain a complete dissolution of the precipitates which are only reduced in size but retain their original irregular shape. Only solutioning at 1245 °C it was possible to dissolve γ' elongated particles completely. These, during the controlled cooling stage, precipitated in a well-organized and regular array of cuboids. Noteworthy, the size of the carbides is drastically reduced if compared with the as-built samples, which were directly subjected to the heat treatment cycle.

Table 3 summarize the most important statistical data related to γ' and carbides populations in the as-built and after HIP respectively. As mentioned before γ' was not measured in the as-built state since it was not detectable using a scanning electron microscope. On the other hand, this was possible for carbides, despite their extremely small size.

All the other metallurgical states are represented in Fig. 8. As shown in the plot, γ' volume fraction ranges between 65% and 73%.

As the solution temperature increases, an higher fraction of particles is obtained at the end of the heating cycle. As the directly solutioned (DS) samples are concerned, a slightly lower volume fraction was assessed. This could be explained considering that, after HIPping, the material is more homogeneous making solution process easier. Noteworthy, the precipitated γ' becomes smaller as the solution temperature is increased, indicating again a more effective treatment. In accordance with the previous observation, γ' is slightly larger in directly solutioned samples, which is compliant with a more difficult dissolution of the precipitates. Besides, carbide size of HIPed and solution samples remains stable within the observed range of solutioning temperatures. Despite this, a slight increase in their volume fraction was evidenced as well. Interestingly, directly solutioned samples show three times larger carbides, which are already observable at lowest solutioning temperature in a volume fraction close to a 3%.

As can be expected also hardness was affected by the solution temperature. Fig. 9 shows the results.

The as-built state is characterized by the highest hardness. This is reasonably correlated to the extremely high residuals stress state

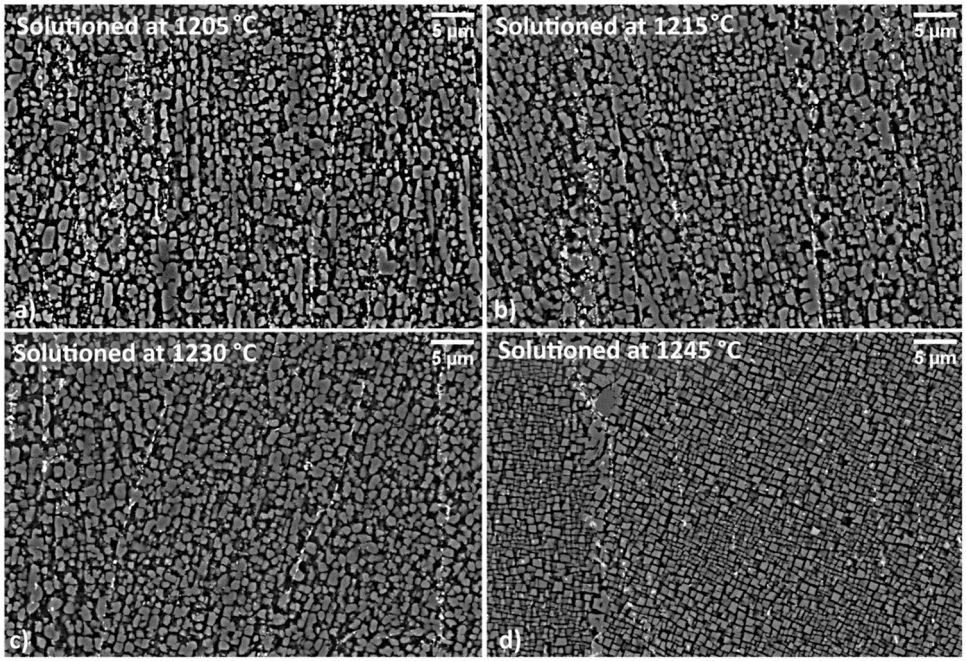

Fig. 7. Backscattered electron detector was used to assess the precipitates obtained at different solution temperature. Solution was performed at a) 1205, b) 1215 °C, c) 1230 °C and d) 1245 °C. All the other treatment parameters are fixed.

Table 3
Most significant statistical data collected after image analysis applied to γ' and carbides.

Metallurgical condition	γ' fraction [%]	γ ' average size [nm]	Carbides fraction [%]	Carbides average size [nm]
As-built	Not mesurable	Not mesurable	1.14 ± 0.55	65 ± 58
HIPped	62 ± 2	904 ± 400	1.81 ± 0.41	98 ± 72

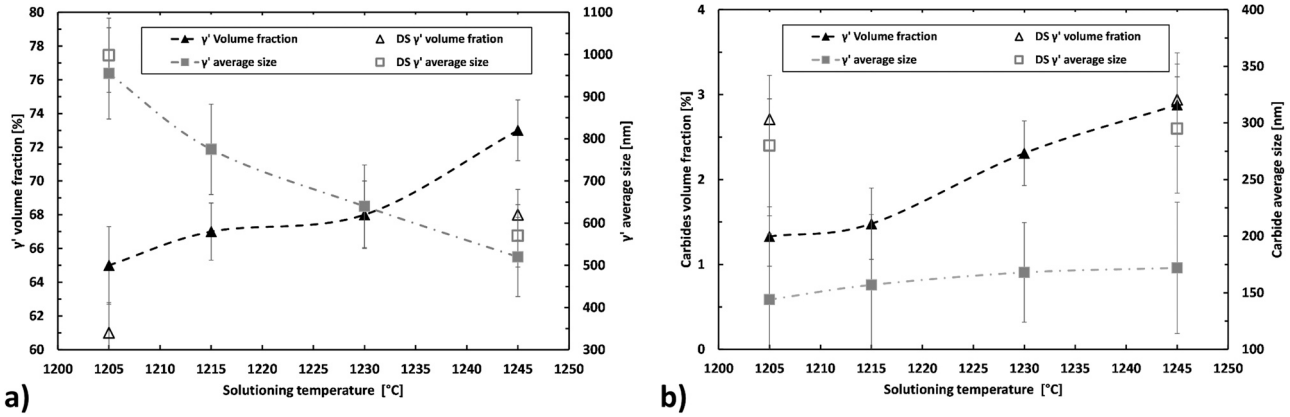

Fig. 8. Volume fraction and average size of γ' a) and carbides b). empty symbols refer to directly solutioned states.

brought by the building process. So, as an effect of hipping, most of the residual stresses are dissipated and, despite the γ' precipitation, hardness strongly decreases. Directly solutioned samples, (indicated as DS) are always softer than the hipped and solutioned (H+S) ones. The increase of the solution temperature leads to the precipitation of finer particles with a more effective reinforcing systems. This is valid as long as the γ' solvus temperature is not overcome. At higher temperatures, as in the 1245 °C case, hardness drops due to the grain coarsening effect. So, despite the higher γ' fraction and its smaller size, the coarsening effect was more impacting towards hardness. This must not be interpreted as a limiting factor since the second aging treatment may catch up with this seeming deficit. Moreover, considering the final application of this type of material, i.e., high temperature application, allowing a larger grain size may be of extreme help in limiting the creep effects. At the same time, having a more regular microstructure will be helpful in enhancing the fatigue resistance as described in literature [43–45] for other alloys reinforced with γ'.

4. Discussion

4.1. Identification of actual γ' solvus temperature

The schematic of Fig. 10 shows as the solution temperature dramatically changes the resulting microstructure of this nickel based alloy, especially when the γ' solvus temperature is overcome.

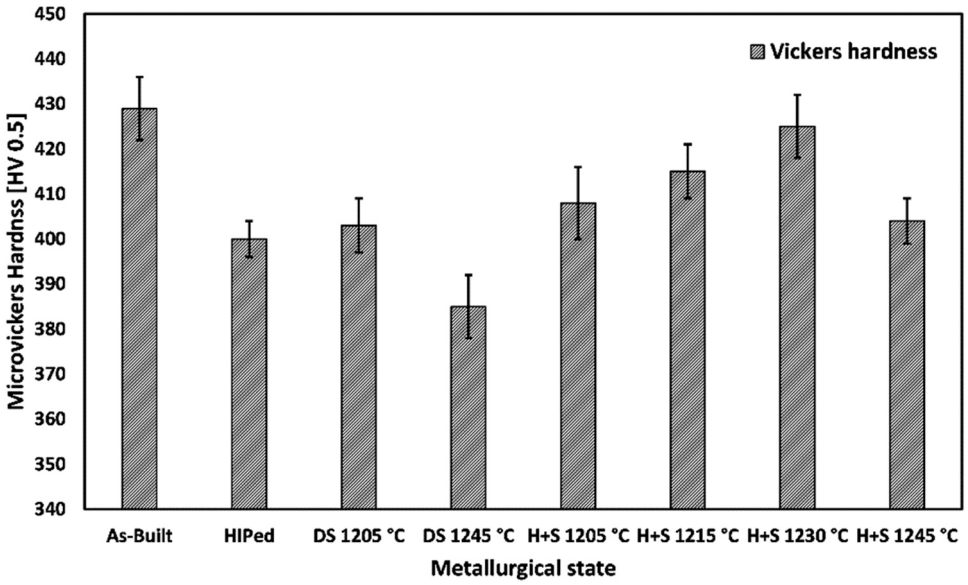

Fig. 9. Vickers hardness measured in after the heat treatment cycle in as-built and post-hip samples.

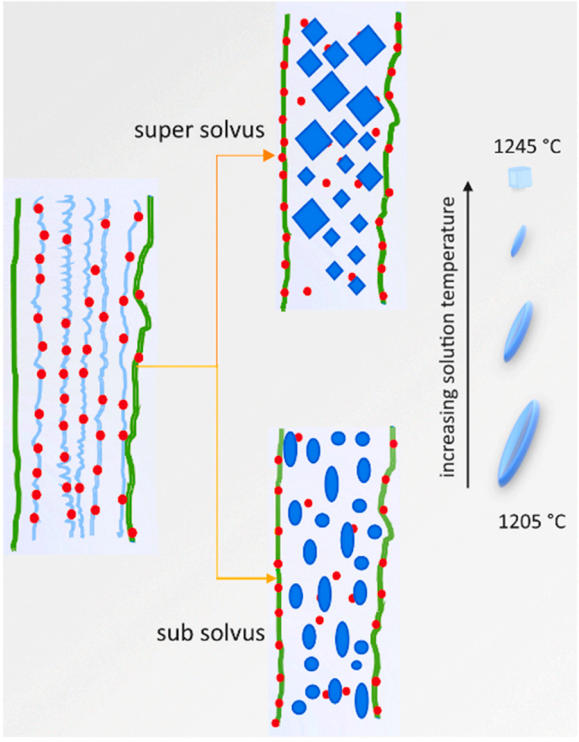

Fig. 10. Schematic showing the effects on matrix and precipitates varying the solutioning temperature.

As soon as the solution treatment is applied (and HIP treatment may be considered as a low-temperature high-pressure solution treatment) the typical dendritic structure is destroyed and substituted with a polycrystalline one. Another important factor regards the γ' formation and shape. Since the second aging treatment was not considered in this study, only primary γ' is present at the end of the heat treatments. For this reason, γ' showed a monomodal distribution in all the samples described in this work as also demonstrated in other literature works on CM247 LC [42]. By comparing Fig. 3, Fig. 5,Fig. 8 and the results in Table 2, it is evident that changing the cooling rate on its own barely impacts on the final size and shape of the particles. In fact, by comparing the HIP samples with the sub-solvus solutioned ones, the resulting particles are still elliptical and only slightly larger. The fact that HIP sample had larger γ' particles is compliant with the slower cooling rate applied, i.e. ca. 3 times slower than that used in the precipitation temperature interval during solutioning. As evidenced in previous paragraph, the size reduction of the particles is mostly caused by an increase of the solution temperature. Or in other words, an enhanced solutioning treatment promotes a competitive nucleation of primary γ', thus limiting its growth. Despite this, only by overcoming the solvus temperature, i.e. 1230–1245 °C γ' is eventually able to precipitate in a cuboidal and ordered fashion.

Finally, the investigation was completed performing EBSD analysis in samples HIPped and heat treated. More specifically, three different solution temperatures were applied i.e. 1215, 1230 and 1245 °C, while all the other parameters were kept unchanged. Fig. 11 shows the progressive recrystallization process underling the slight, almost negligible, grain coarsening observable in the γ' sub-solvus temperature window. The effect is considerably more impacting as soon as the treatment is performed without relying on the precipitates pinning effect i.e. above 1230 °C.

According to the EBSD analysis, around 55% and 54% of low-angle grain boundaries (i.e. with a degree of misorientation lower than 10°) population are reported for the solutioned samples at 1215 °C and 1230 °C, respectively. The very high content of low-angle grain boundaries indicates the limited activation of recrystallization mechanisms that usually involve their drastical reduction due to the apparent stability of the microstructure for solutioning temperature below γ'. However, the low-angle grain boundaries drop under 5% when subjected to heat treatment at 1245 °C, which is above the γ' solvus temperature. Although the grains are still elongated along the building direction, recrystallization mechanisms occurred, generating a microstructure closer to an equiaxial one. Moreover, this is also evident from the formation of new grains, as displayed in Fig. 11c.

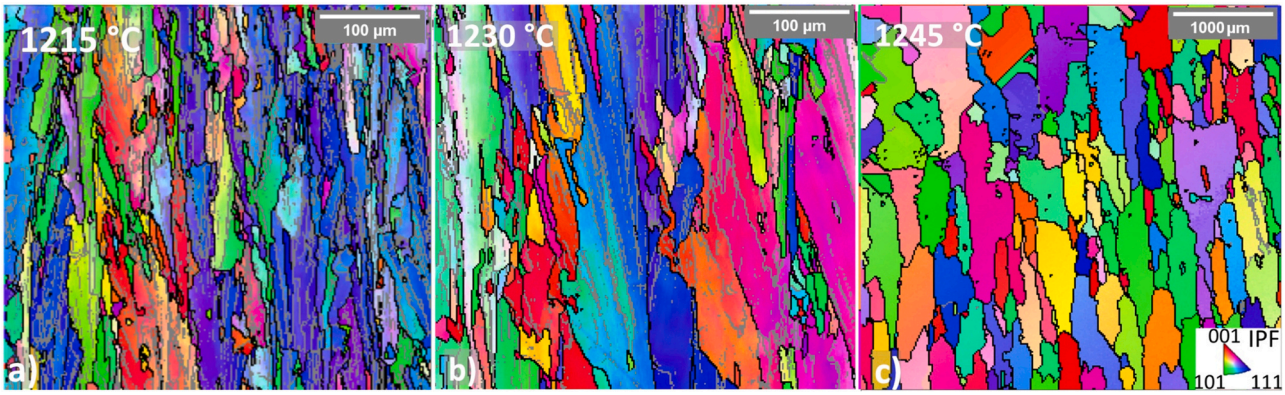

Fig. 11. EBSD maps performed on samples with different solution temperatures applied at: a) 1215 °C b) 1230 and c) 1245 °C. The low-angle grain boundaries (< 10°) are highlighted in gray while the high-angle grain boundaries are pointed out in black.

5. Conclusions

In this work, different heat treatments were applied to SLM CM247LC. More specifically, the alloy was assessed after HIPping and after being solutioned at different temperature and aged. As thoroughly discussed in this work, the principal aim of this research work was tailoring the material microstructure by optimizing the solutioning stage, being this very step the one that will mostly affect its final properties. Next, the main findings are listed as follows.

- 1205 °C i.e. the lowest solutioning temperature investigated here, proved to be sufficient to promote an initial recrystallization process by eliminating the dendritic microstructure of the as-built material.
- HIP process was extremely effective in removing SLM flaws, and positively acted in stabilizing the microstructure leading to:
  a) An enhancement of the solution process in the heat treatment stage: γ' volume fraction was higher and precipitates were finer, giving a higher hardness level.
  b) A strong limitation to carbide coarsening during the solution treatment.
- By gradually increasing the solution temperature a finer γ' population can be obtained but only overcoming its solvus point, a really ordered and fine precipitation can be achieved
- 1245 °C solutioning temperature proved to be a good compromise for the heat treatment of component which will be applied in environment characterized by demanding creep condition thanks to the more regular γ' precipitation and a larger grain size.

CRediT authorship contribution statement

Emilio Bassini: Conceptualization, Methodology, Writing – original draft preparation, Writing – review & editing. **Antonio Sivo** and **Pietro Martelli**, **Ewa Rajczak**, **Giulio Marchese**, **Calignano Flaviana:** Data curation, sample printing and Software. **Daniele Ugues**, **Sara Biamino:** Supervision.

Declaration of Competing Interest

The authors declare that they have no known competing financial interests or personal relationships that could have appeared to influence the work reported in this paper.

Acknowledgement

This project has received founding from the Clean Sky 2 Joint Undertaking under the European Union's Horizon 2020 Research and Innovation Program under grant agreement No. 821274.

References

[1] J.E. MacDonald, R.H.U. Khan, M. Aristizabal, K.E.A. Essa, M.J. Lunt, M.M. Attallah, Influence of powder characteristics on the microstructure and mechanical properties of HIPped CM247LC Ni superalloy, Mater. Des. 174 (2019) 107796, https://doi.org/10.1016/j.matdes.2019.107796
[2] C. Yang, Y. Xu, H. Nie, X. Xiao, G. Jia, Z. Shen, Effects of heat treatments on the microstructure and mechanical properties of Rene 80, Mater. Des. 43 (2013) 66–73, https://doi.org/10.1016/j.matdes.2012.06.039
[3] Y. Xu, Q. Jin, X. Xiao, X. Cao, G. Jia, Y. Zhu, H. Yin, Strengthening mechanisms of carbon in modified nickel-based superalloy Nimonic 80A, Mater. Sci. Eng. A 528 (2011) 4600–4607, https://doi.org/10.1016/j.msea.2011.02.072
[4] Y. Xu, C. Yang, X. Xiao, X. Cao, G. Jia, Z. Shen, Strengthening behavior of Al and Ti elements at room temperature and high temperature in modified Nimonic 80A, Mater. Chem. Phys. 134 (2012) 706–715, https://doi.org/10.1016/j.matchemphys.2012.03.055
[5] J.P. Collier, S.H. Wong, J.K. Tien, J.C. Phillips, J.K. Tein, Effect of varying Al, Ti, and Nb content on the phase stability of Inconel 718, Metall. Trans. A Phys. Metall. Mater. Sci. 19 A (1988) 1657–1666, https://doi.org/10.1007/BF02645133
[6] G. Marchese, E. Bassini, S. Parizia, D. Manfredi, D. Ugues, M. Lombardi, P. Fino, S. Biamino, Role of the chemical homogenization on the microstructural and mechanical evolution of prolonged heat-treated laser powder bed fused Inconel 625, Mater. Sci. Eng. A. 796 (2020) 140007, https://doi.org/10.1016/j.msea.2020.140007
[7] W.R. Sun, J.H. Lee, S.M. Seo, S.J. Choe, Z.Q. Hu, The eutectic characteristic of MC-type carbide precipitation in a DS nickel-base superalloy, Mater. Sci. Eng. A 271 (1999) 143–149, https://doi.org/10.1016/s0921-5093(99)00189-6
[8] G. Marchese, X. Garmendia Colera, F. Calignano, M. Lorusso, S. Biamino, P. Minetola, D. Manfredi, Characterization and comparison of Inconel 625 processed by selective laser melting and laser metal deposition, Adv. Eng. Mater. 19 (2017) 2–6, https://doi.org/10.1002/adem.201600635
[9] G. Marchese, E. Bassini, A. Aversa, M. Lombardi, D. Ugues, P. Fino, S. Biamino, Microstructural evolution of post-processed Hastelloy X alloy fabricated by laser powder bed fusion, Materials 12 (2019), https://doi.org/10.3390/ma12030486
[10] M. Calandri, S. Yin, B. Aldwell, F. Calignano, R. Lupoi, D. Ugues, Texture and microstructural features at different length scales in Inconel 718 produced by selective laser melting, Materials 12 (2019), https://doi.org/10.3390/ma12081293
[11] G. Marchese, E. Bassini, M. Calandri, E.P. Ambrosio, F. Calignano, M. Lorusso, D. Manfredi, M. Pavese, S. Biamino, P. Fino, Microstructural investigation of as-fabricated and heat-treated Inconel 625 and Inconel 718 fabricated by direct metal laser sintering: contribution of Politecnico di Torino and Istituto Italiano di Tecnologia (IIT) di Torino, Met. Powder Rep. 71 (2016) 273–278, https://doi.org/10.1016/j.mprp.2016.06.002
[12] E. Bassini, G. Marchese, A. Aversa, Tailoring of the microstructure of laser powder bed fused inconel 718 using solution annealing and aging treatments, Metals 11 (2021) 1–17, https://doi.org/10.3390/met11060921
[13] A. Aversa, G. Marchese, E. Bassini, Directed energy deposition of aisi 316l stainless steel powder: effect of process parameters, Metals 11 (2021) 932, https://doi.org/10.3390/met11060932
[14] M.T. Rush, P.A. Colegrove, Z. Zhang, D. Broad, Liquation and post-weld heat treatment cracking in Rene 80 laser repair welds, J. Mater. Process. Technol. 212 (2012) 188–197, https://doi.org/10.1016/j.jmatprotec.2011.09.001
[15] G. Marchese, S. Parizia, A. Saboori, D. Manfredi, M. Lombardi, P. Fino, D. Ugues, S. Biamino, The influence of the process parameters on the densification and microstructure development of laser powder bed fused inconel 939, Metals 10 (2020) 1–19, https://doi.org/10.3390/met10070882
[16] M.J. Donachie, S.J. Donachie, Superalloys a Technical Guide, 2002. ⟨https://doi.org/10.1361/stgs2002p001⟩.
[17] L.N. Carter, M.M. Attallah, R.C. Reed, Laser powder bed fabrication of nickel-base superalloys: influence of parameters; characterisation, quantification and mitigation of cracking, Superalloys 2012 (2012) 577–586, https://doi.org/10.1002/9781118516430.ch64

[18] D. Grange, J.D. Bartout, B. Macquaire, C. Colin, Processing a non-weldable nickel-base superalloy by Selective Laser Melting: role of the shape and size of the melt pools on solidification cracking, Materialia 12 (2020) 100686, https://doi.org/10.1016/j.mtla.2020.100686
[19] G. Bidron, A. Doghri, T. Malot, F. Fournier-dit-Chabert, M. Thomas, P. Peyre, Reduction of the hot cracking sensitivity of CM-247LC superalloy processed by laser cladding using induction preheating, J. Mater. Process. Technol. 277 (2020) 116461, https://doi.org/10.1016/j.jmatprotec.2019.116461
[20] M. Gerstgrasser, M. Cloots, J. Stirnimann, K. Wegener, Focus shift analysis, to manufacture dense and crack-free SLM-processed CM247LC samples, J. Mater. Process. Technol. 289 (2021) 116948, https://doi.org/10.1016/j.jmatprotec.2020.116948
[21] Z.A. Sentyurina, F.A. Baskov, P.A. Loginov, Y.Y. Kaplanskii, A.V. Mishukov, I.A. Logachev, M.Y. Bychkova, E.A. Levashov, A.I. Logacheva, The effect of hot isostatic pressing and heat treatment on the microstructure and properties of EP741NP nickel alloy manufactured by laser powder bed fusion, Addit. Manuf. (2020) 101629, https://doi.org/10.1016/j.addma.2020.101629
[22] J. Radavich, D. Furrer, Assessment of Russian P/M Superalloy EP741NP, in: Superalloys 2004 TMS, 2004: pp. 381–390.
[23] E. Bassini, G. Cattano, G. Marchese, S. Biamino, D. Ugues, M. Lombardi, G. Vallillo, B. Picqué, Study of the effects of aging treatment on astroloy processed via hot isostatic pressing, Materials 12 (2019) 1517, https://doi.org/10.3390/ma12091517
[24] E. Bassini, U. Galech, T. Soria, M. Aristizabal, I. Iturriza, S. Biamino, D. Ugues, Effect of the particle size distribution on physical properties, composition, and quality of gas atomized Astroloy powders for HIP application, J. Alloy. Compd. 890 (2022) 161631, https://doi.org/10.1016/j.jallcom.2021.161631
[25] E. Bassini, G. Marchese, G. Cattano, M. Lombardi, S. Biamino, D. Ugues, G. Vallillo, B. Picqué, Influence of solutioning on microstructure and hardness of hot isostatically pressed Astroloy, J. Alloy. Compd. 723 (2017) 1082–1090, https://doi.org/10.1016/j.jallcom.2017.06.332
[26] Y.L. Kuo, T. Nagahari, K. Kakehi, The effect of post-processes on the microstructure and creep properties of Alloy718 built up by selective laser melting, Materials 11 (2018) 996, https://doi.org/10.3390/ma11060996
[27] C.N. Wei, H.Y. Bor, L. Chang, Effect of hot isostatic pressing on microstructure and mechanical properties of CM-681LC nickel-base superalloy using microcast, Mater. Trans. 49 (2008) 193–201, https://doi.org/10.2320/matertrans.MER2007088
[28] R. Baldan, R.L.P. Rocha, R.B. Tomasiello, C.A. Nunes, A.M.S. Costa, M.J.R. Barboza, G.C. Coelho, R. Rosenthal, Solutioning and aging of MAR-M247 nickel-based superalloy, J. Mater. Eng. Perform. 22 (2013) 2574–2579, https://doi.org/10.1007/s11665-013-0565-4
[29] X. Wang, L.N. Carter, B. Pang, M.M. Attallah, M.H. Loretto, Microstructure and yield strength of SLM-fabricated CM247LC Ni-Superalloy, Acta Mater. 128 (2017) 87–95, https://doi.org/10.1016/j.actamat.2017.02.007
[30] H. Mughrabi, The importance of sign and magnitude of γ/γ′ lattice misfit in superalloys - with special reference to the new γ′-hardened cobalt-base superalloys, Acta Mater. 81 (2014) 21–29, https://doi.org/10.1016/j.actamat.2014.08.005
[31] M.M. Barjesteh, S.M. Abbasi, K. Zangeneh Madar, K. Shirvani, The effect of heat treatment on characteristics of the gamma prime phase and hardness of the nickel-based superalloy Rene ® 80, Mater. Chem. Phys. 227 (2019) 46–55, https://doi.org/10.1016/j.matchemphys.2019.01.038
[32] I.S. Kim, B.G. Choi, J.E. Jung, J. Do, W.Y. Seok, Y.H. Lee, I.Y. Jeong, Effect of heat treatment on microstructural evolution and creep behaviors of a conventionally cast nickel-based superalloy, Mater. Charact. 165 (2020) 110378, https://doi.org/10.1016/j.matchar.2020.110378
[33] E. Bassini, G. Marchese, G. Cattano, M. Lombardi, S. Biamino, D. Ugues, G. Vallillo, B. Picqué, Influence of solutioning on microstructure and hardness of hot isostatically pressed Astroloy, J. Alloy. Compd. 723 (2017) 1082–1090, https://doi.org/10.1016/j.jallcom.2017.06.332
[34] E. Bassini, L. Iannucci, M. Lombardi, S. Biamino, D. Ugues, G. Vallillo, B. Picqué, Net shape HIPping of a Ni-superalloy: a study of the influence of an as-leached surface on mechanical properties, J. Mater. Process. Technol. 271 (2019) 476–487, https://doi.org/10.1016/j.jmatprotec.2019.04.027
[35] E. Bassini, M. Calandri, G. Marchese, A. Saboori, A. Aversa, M. Lombardi, D. Ugues, S. Biamino, P. Fino, Effect of a Fine Tailored Heat Treatment on the Microstructure and Hardness of Inconel 718 Produced via Selective Laser Melting (SLM), (n.d.), 718.
[36] T.M. Pollock, S. Tin, Nickel-based superalloys for advanced turbine engines: chemistry, microstructure, and properties, J. Propuls. Power 22 (2006) 361–374, https://doi.org/10.2514/1.18239
[37] M. Calandri, D. Manfredi, F. Calignano, E.P. Ambrosio, S. Biamino, R. Lupoi, D. Ugues, Solution treatment study of Inconel 718 produced by SLM additive technique in view of the oxidation resistance, Adv. Eng. Mater. 20 (2018) 1–16, https://doi.org/10.1002/adem.201800351
[38] J. Xu, H. Gruber, R. Lin Peng, J. Moverare, A novel γ′-strengthened nickel-based superalloy for laser powder bed fusion, Materials 13 (2020) 4930, https://doi.org/10.3390/ma13214930
[39] K. Kakehi, Effect of primary and secondary precipitates on creep strength of Ni-base superalloy single crystals, Mater. Sci. Eng. A 278 (2000) 135–141, https://doi.org/10.1016/S0921-5093(99)00579-1
[40] M. Aghaie-Khafri, M. Hajjavady, The effect of thermal exposure on the properties of a Ni-base superalloy, Mater. Sci. Eng. A 487 (2008) 388–393, https://doi.org/10.1016/j.msea.2007.11.010
[41] M. Mostafaei, S.M. Abbasi, Solutioning and solidification process control in Ta-modified CM247 LC superalloy, J. Mater. Process. Technol. 231 (2016) 113–124, https://doi.org/10.1016/j.jmatprotec.2015.12.021
[42] V.D. Divya, R. Muñoz-Moreno, O.M.D.M. Messé, J.S. Barnard, S. Baker, T. Illston, H.J. Stone, Microstructure of selective laser melted CM247LC nickel-based superalloy and its evolution through heat treatment, Mater. Charact. 114 (2016) 62–74, https://doi.org/10.1016/j.matchar.2016.02.004
[43] L. Whitmore, M.R. Ahmadi, L. Guetaz, H. Leitner, E. Povoden-Karadeniz, M. Stockinger, E. Kozeschnik, The microstructure of heat-treated nickel-based superalloy 718Plus, Mater. Sci. Eng. A 610 (2014) 39–45, https://doi.org/10.1016/j.msea.2014.05.022
[44] A.R.P. Singh, S. Nag, J.Y. Hwang, G.B. Viswanathan, J. Tiley, R. Srinivasan, H.L. Fraser, R. Banerjee, Influence of cooling rate on the development of multiple generations of γ ′ precipitates in a commercial nickel base superalloy, Mater. Charact. 62 (2011) 878–886, https://doi.org/10.1016/j.matchar.2011.06.002
[45] C.L. Qiu, M.M. Attallah, X.H. Wu, P. Andrews, Influence of hot isostatic pressing temperature on microstructure and tensile properties of a nickel-based superalloy powder, Mater. Sci. Eng. A 564 (2013) 176–185, https://doi.org/10.1016/j.msea.2012.11.084